Kinetic transverse dispersion relation for relativistic magnetized electron-positron plasmas with Maxwell-Jüttner velocity distribution functions

Rodrigo A. López, Pablo S. Moya, Víctor Muñoz, Adolfo F. Viñas, and J. Alejandro Valdivia

Citation: Physics of Plasmas (1994-present) **21**, 092107 (2014); doi: 10.1063/1.4894679
View online: http://dx.doi.org/10.1063/1.4894679
View Table of Contents: http://scitation.aip.org/content/aip/journal/pop/21/9?ver=pdfcov
Published by the AIP Publishing

Kinetic transverse dispersion relation for relativistic magnetized electron-positron plasmas with Maxwell-Jüttner velocity distribution functions

Rodrigo A. López,[1] Pablo S. Moya,[2,3] Víctor Muñoz,[4] Adolfo F. Viñas,[2] and J. Alejandro Valdivia[4,5]
[1]*Departamento de Física, Facultad de Ciencias Físicas y Matemáticas, Universidad de Concepción, Concepción, Chile*
[2]*NASA Goddard Space Flight Center, Heliophysics Science Division, Geospace Physics Laboratory, Mail Code 673, Greenbelt, Maryland 20771, USA*
[3]*Department of Physics, Catholic University of America, Washington DC, DC 20064, USA*
[4]*Departamento de Física, Facultad de Ciencias, Universidad de Chile, Casilla 653, Santiago, Chile*
[5]*Centro para el Desarrollo de la Nanociencia y la Nanotecnología, CEDENNA, Santiago, Chile*

(Received 8 May 2014; accepted 19 August 2014; published online 9 September 2014)

We use a kinetic treatment to study the linear transverse dispersion relation for a magnetized isotropic relativistic electron-positron plasma with finite relativistic temperature. The explicit linear dispersion relation for electromagnetic waves propagating along a constant background magnetic field is presented, including an analytical continuation to the whole complex frequency plane for the case of Maxwell-Jüttner velocity distribution functions. This dispersion relation is studied numerically for various temperatures. For left-handed solutions, the system presents two branches, the electromagnetic ordinary mode and the Alfvén mode. In the low frequency regime, the Alfvén branch has two dispersive zones, the normal zone (where $\partial\omega/\partial k > 0$) and an anomalous zone (where $\partial\omega/\partial k < 0$). We find that in the anomalous zone of the Alfvén branch, the electromagnetic waves are damped, and there is a maximum wave number for which the Alfvén branch is suppressed. We also study the dependence of the Alfvén velocity and effective plasma frequency with the temperature. We complemented the analytical and numerical approaches with relativistic full particle simulations, which consistently agree with the analytical results. © *2014 AIP Publishing LLC*.
[http://dx.doi.org/10.1063/1.4894679]

I. INTRODUCTION

Relativistic electron-positron plasmas have received much attention during the last decades. They are relevant in several environments of astrophysical and laboratory nature, such as accretion disks,[1–3] models of early universe,[4,5] pulsar magnetospheres,[6,7] hypothetical quark stars,[8] ultraintense lasers,[9] and laboratory and tokamak plasmas.[10,11] In several of the physical systems mentioned above, relativistic effects and temperature play an important role, thus, it is fundamental to understand wave propagation modes in relativistic plasmas with temperature, in particular, kinetic effects. Even though relativistic fluid models have successfully taken into account thermal[12] and non-linear[13,14] effects in the propagation of electromagnetic waves in relativistic plasmas, a kinetic model is needed to have a better understanding of the wave propagation, as effects such as wave-particle interactions are expected to modify it.

Within this context, Domínguez *et al.*[15] studied the propagation of waves in relativistically magnetized electron-positron plasmas based on the one dimensional relativistic Vlasov equation along the direction of the background magnetic field, and considering the plasma as a fluid in the perpendicular plane.[16,17] In their study, comparing with the fluid model of Asenjo *et al.*,[12] Domínguez *et al.*[15] found that both models agree in the dependence of the plasma frequency and Alfvén speed on temperature, but kinetic effects increase the plasma frequency and decrease the Alfvén speed for a given temperature. However, in Domínguez *et al.*[15] kinetic effects are considered only in the direction of propagation of the waves and damping effects are not taken into account.

On the other hand, Schlickeiser[18] and Lazar and Schlickeiser[19,20] have developed a model to express the fully kinetic dispersion relation for waves propagating parallel to the mean magnetic field, as a one dimensional integral depending only on the Lorentz factor and the temperature. In the case of isotropic velocity distribution functions, Lazar and Schlickeiser[20] describe both growing and the damped waves, by analytical continuation in the whole complex frequency plane. They found important relativistic corrections, in particular, for pair plasmas (e.g., electron-positron plasmas) and nonisothermal plasmas, in which relativistic effects play an important role at low frequencies even for nonrelativistic temperatures. This particular theoretical technique has been recently used in the study of spontaneous electromagnetic fluctuations in unmagnetized[21–24] and magnetized[25] plasmas.

In the present manuscript, we have applied the model by Lazar and Schilckeiser[20] to obtain the complex dispersion relation in the case of circularly polarized waves propagating in the direction of the mean field, in a relativistic electron-positron plasma modeled with a Maxwell-Jüttner velocity distribution function. We thus generalize the work of

Domínguez *et al.*, by considering kinetic effects on all spatial directions, not only along the background magnetic field. We calculate the explicit analytic continuation in the complex plane and compute the complex frequencies as a function of the wave number for various values of the temperature and plasma beta parameter. In addition, we compare our theoretical calculations with full particle relativistic *Particle in Cell* (PIC) simulations to test our results.

This paper is organized as follows. In Sec. II, the linear dispersion relation is derived, including the proper analytical continuation from positive to negative imaginary parts of the frequencies. In Sec. III, the dispersion relation is solved numerically and its main features are discussed, whereas in Sec. IV, we complement the analytical and numerical approaches with the performance of relativistic PIC simulations in the stable regime of the plasma under various thermal conditions. Finally, in Sec. V, our results are summarized and conclusions are outlined.

II. LINEAR DISPERSION RELATION

Let us start from the relativistic Vlasov equation

$$\frac{\partial f_j}{\partial t}+\vec{v}\cdot\frac{\partial f_j}{\partial \vec{x}}+q_j\left(\vec{E}+\frac{\vec{v}}{c}\times\vec{B}\right)\cdot\frac{\partial f_j}{\partial \vec{p}}=0\,, \tag{1}$$

where q_j is the charge, m_j is the mass of each particle species, j is the species index, c is the light speed, and $\vec{p}$ is the relativistic momentum.

The linear dispersion relation is derived from Eq. (1). For waves propagating parallel to the background magnetic field $\vec{B}_0=B_0\hat{z}$, the transverse dispersion relation is given by[19,20]

$$\Lambda^{+}_{R,L}=1-\frac{c^2k^2}{\omega^2}+\pi\sum_j\omega^2_{p,j}\int_{-\infty}^{\infty}dp_z\int_0^{\infty}dp_\perp\frac{p_\perp^2}{\gamma\omega-kp_z/m\pm\Omega_j}\times\left[\left(\omega-\frac{kp_z}{m\gamma}\right)\frac{\partial f_j^{(0)}}{\partial p_\perp}+\frac{kp_\perp}{m\gamma}\frac{\partial f_j^{(0)}}{\partial p_z}\right]=0\,, \tag{2}$$

where $\omega_{p,j}=\sqrt{4\pi q_j^2 n_j/m}$ is the plasma frequency, $\Omega_j=q_jB_0/(mc)$ is the cyclotron frequency for the species j, and $f_j^{(0)}(p_z,p_\perp)$ is the one-particle distribution function of the species j that depends on the relativistic momentum p_z and $p_\perp$ parallel and perpendicular to the background field, respectively. Subscripts R and L in Λ, are the labels for the right and left-handed polarized waves, respectively. Notice that right-handed (left-handed) polarized waves correspond to the plus (minus) sign in the resonant denominator $\gamma\omega-kp_z/m\pm\Omega_j$ in Eq. (2). The wave frequency is a complex number, which we write as $\omega=\omega_r+i\Gamma$, where ω_r is its real part and Γ is its imaginary part. The superindex $+$ in Λ indicates that the dispersion relation Eq. (2) is only valid for $\Gamma>0$. Finally, $\gamma=\sqrt{1+(p_\perp/mc)^2+(p_z/mc)^2}$ is the relativistic Lorentz factor.

We can rewrite Eq. (2) using the transformation

$$s=p_z/(mc)\,, \tag{3}$$

$$\gamma=\sqrt{1+p_\perp^2/(mc)^2+p_z^2/(mc)^2}\,, \tag{4}$$

where the determinant of the Jacobian matrix is

$$\det \mathrm{Jc}=\frac{\gamma(mc)^2}{\sqrt{\gamma^2-1-s^2}}\,. \tag{5}$$

Then, Eq. (2) becomes

$$\Lambda^{+}_{R,L}=1-\frac{c^2k^2}{\omega^2}-\pi\sum_j(m_jc)^3\frac{\omega_{pj}^2}{\omega^2}\times\int_1^{\infty}d\gamma\int_{-\sqrt{\gamma^2-1}}^{\sqrt{\gamma^2-1}}ds\left(\frac{\partial f_j^{(0)}}{\partial s}+\frac{\omega}{ck}\frac{\partial f_j^{(0)}}{\partial\gamma}\right)\times\frac{\gamma^2-1-s^2}{s-\gamma\omega/(ck)\mp\Omega_j/(ck)}=0\,. \tag{6}$$

We are interested in studying a relativistic Maxwell-Jüttner distribution function[26] given by

$$f_j^{(0)}(\gamma)=\frac{\mu_j}{4\pi(m_jc)^3K_2(\mu_j)}\,e^{-\mu_j\gamma}\,, \tag{7}$$

which is an isotropic distribution function $f_j^{(0)}=f_j^{(0)}(\gamma)$. In Eq. (7), $\mu_j=mc^2/(k_BT_j)$ is a dimensionless parameter related to the plasma temperature and K_2 is the modified Bessel function of order 2. Then, Eq. (6) reduces to

$$\Lambda^{+}_{R,L}=1-\frac{1}{z^2}-\pi\sum_j(m_jc)^3\frac{\omega_{pj}^2}{c^2k^2z}\int_1^{\infty}d\gamma\frac{df_j^{(0)}}{d\gamma}\times\int_{-\sqrt{\gamma^2-1}}^{\sqrt{\gamma^2-1}}ds\,\frac{\gamma^2-1-s^2}{s-\gamma z\mp t_j}=0\,, \tag{8}$$

where we have defined $z=\omega/(ck)$ and $t_j=\Omega_j/(ck)$.

Following Ref. 20, we define

$$L^{+}_{R,L;j}(\gamma,z,t)=\int_{-\sqrt{\gamma^2-1}}^{\sqrt{\gamma^2-1}}ds\,\frac{\gamma^2-1-s^2}{s-\gamma z\mp t_j}\,, \tag{9}$$

and using the substitution $(s\mp t_j)/\gamma=\xi$, the integral becomes

$$L^{+}_{R,L;j}(\gamma,z,t)=\int_{-\sqrt{1-\gamma^{-2}}\mp t_j/\gamma}^{\sqrt{1-\gamma^{-2}}\mp t_j/\gamma}d\xi\,\frac{\gamma^2-1-t_j^2-\gamma^2\xi^2\mp 2t_j\gamma\xi}{\xi-z}\,. \tag{10}$$

Furthermore, we can reduce this integral, Eq. (10), in the form

$$L^{+}_{R,L;j}(\gamma,z,t)=[(1-z^2)\gamma^2\mp 2zt_j\gamma-(1+t_j^2)]J^{+}_{R,L;j}(\gamma,z,t)-2(z\gamma\pm t_j)\sqrt{\gamma^2-1}\,, \tag{11}$$

where we have defined

$$J^{+}_{R,L;j}(\gamma,z,t)=\int_{-\sqrt{1-\gamma^{-2}}\mp t_j/\gamma}^{\sqrt{1-\gamma^{-2}}\mp t_j/\gamma}d\xi\,\frac{1}{\xi-z}\,. \tag{12}$$

Finally, using these definitions, the dispersion relation, Eq. (8), can be rewritten as

$$\Lambda^{+}_{R,L} = 1 - \frac{1}{z^2} + 2\pi \sum_j (m_j c)^3 \frac{\omega^2_{pj}}{c^2 k^2 z} \int_1^\infty d\gamma \, \frac{df^{(0)}_j}{d\gamma} (\gamma z \pm t_j) \sqrt{\gamma^2 - 1}$$
$$-\pi \sum_j (m_j c)^3 \frac{\omega^2_{pj}}{c^2 k^2 z} \int_1^\infty d\gamma \, \frac{df^{(0)}_j}{d\gamma} J^{+}_{R,L;j}(\gamma, z, t) \left[(1 - z^2)\gamma^2 \mp 2 z t_j \gamma - \left(1 + t_j^2\right) \right] = 0 \,, \tag{13}$$

i.e., we have reduced the dispersion relation into a one-dimensional complex integral.

In the case of an electron-positron plasma, we have $m_e = m_p = m$, and considering that both species have equal temperature, so $\mu_e = \mu_p = \mu$, the dispersion relation becomes

$$\Lambda^{+}_{R,L} = 1 - \frac{1}{z^2} - \frac{\omega^2_{pe}\mu}{c^2 k^2} + \frac{\omega^2_{pe}\mu^2}{4K_2(\mu)} \frac{1}{c^2 k^2 z} \left\{ \int_1^\infty d\gamma \, e^{-\mu\gamma} J^{+}_{R,L;e}(\gamma, z, t) \left[(1 - z^2)\gamma^2 \pm 2 z t \gamma - (1 + t^2) \right] \right.$$
$$\left. + \int_1^\infty d\gamma \, e^{-\mu\gamma} J^{+}_{R,L;p}(\gamma, z, t) \left[(1 - z^2)\gamma^2 \mp 2 z t \gamma - (1 + t^2) \right] \right\} = 0 \,. \tag{14}$$

Here, we have used the identities

$$\int_1^\infty \sqrt{\gamma^2 - 1} \, e^{-\mu\gamma} d\gamma = \frac{K_1(\mu)}{\mu} \,, \tag{15}$$

$$\int_1^\infty \gamma \sqrt{\gamma^2 - 1} \, e^{-\mu\gamma} d\gamma = \frac{K_2(\mu)}{\mu} \,, \tag{16}$$

where K_1 is the modified Bessel function of order 1.

Due to the mass symmetry between electrons and positrons, Eq. (14) is symmetric with respect to the reflections $k \to -k$, and the change between left- and right-handed polarized waves is equivalent to the reflection $\omega \to -\omega$. From now on, we will study the dispersion relation of left-handed circularly polarized electromagnetic waves, in which case the dispersion relation, Eq. (14), yields

$$\Lambda^{+}_{L} = 1 - \frac{1}{z^2} - \frac{\omega^2_{pe}\mu}{c^2 k^2} + \frac{\omega^2_{pe}\mu^2}{4K_2(\mu)} \frac{1}{c^2 k^2 z} \left\{ \int_1^\infty d\gamma \, e^{-\mu\gamma} J^{+}_{L;e}(\gamma, z, t) \left[(1 - z^2)\gamma^2 - 2 z t \gamma - (1 + t^2) \right] \right.$$
$$\left. + \int_1^\infty d\gamma \, e^{-\mu\gamma} J^{+}_{L;p}(\gamma, z, t) \left[(1 - z^2)\gamma^2 + 2 z t \gamma - (1 + t^2) \right] \right\} = 0 \,, \tag{17}$$

and the proper definition of $J^{+}_{L,j}$ is given by

$$J^{+}_{L;j}(\gamma, z, t) = \int_{-\sqrt{1-\gamma^{-2}} + t_j/\gamma}^{\sqrt{1-\gamma^{-2}} + t_j/\gamma} d\xi \, \frac{1}{\xi - z} \,. \tag{18}$$

Equation (17) is expected to yield the electromagnetic ordinary and Alfvén modes (this can be seen, for instance, by considering the cold limit). In the case of right-handed waves, $\Lambda^{+}_{R} = 0$, they are expected to correspond to electromagnetic extraordinary and whistler wave modes.

A. Analytical Continuation

The dispersion relation for a relativistic electron-positron plasma [Eq. (17)] is only valid for the upper complex frequency plane $\mathrm{Im}(\omega) = \Gamma > 0$. To find the dispersion relation in the whole complex frequency plane, we have to do the proper analytical continuation to Λ^{-}_{L} for $\Gamma \leq 0$, such that

$$\lim_{\Gamma \to 0^+} \Lambda^{+}_{L} = \lim_{\Gamma \to 0^-} \Lambda^{-}_{L} \,, \tag{19}$$

which is equivalent to finding the analytical continuation of the integral $J^{-}_{L;j}$:

$$\lim_{\Gamma \to 0^+} J^{+}_{L;j} = \lim_{\Gamma \to 0^-} J^{-}_{L;j} \,. \tag{20}$$

We define

$$S_{1j}(\gamma) = \sqrt{1 - \gamma^{-2}} - \frac{t_j}{\gamma} \,, \tag{21}$$

$$S_{2j}(\gamma) = \sqrt{1 - \gamma^{-2}} + \frac{t_j}{\gamma} \,, \tag{22}$$

which are the limits in the integral of Eq. (18) for each species. In the Appendix A, we show the complete derivation of the analytical continuation for the integral of Eq. (18), which fulfills the condition in Eq. (20). Then, for electrons, we have

$$J_{L;e}(\gamma,z,t)=\frac{1}{2}\ln\left\{\frac{\left[\mathrm{Re}(z)-S_{2e}(\gamma)\right]^2+\mathrm{Im}(z)^2}{\left[\mathrm{Re}(z)+S_{1e}(\gamma)\right]^2+\mathrm{Im}(z)^2}\right\}+i\left\{\arctan\left[\frac{S_{2e}(\gamma)-\mathrm{Re}(z)}{\mathrm{Im}(z)}\right]+\arctan\left[\frac{S_{1e}(\gamma)+\mathrm{Re}(z)}{\mathrm{Im}(z)}\right]+\theta_e(\gamma)\right\},\quad(23)$$

with

$$\theta_e(\gamma)=\begin{cases}0, & \mathrm{Re}(z)\le-\sqrt{1+t^2},\\ \pi\sigma\Theta(\gamma-\gamma_{1e})\Theta(\gamma_{2e}-\gamma), & -\sqrt{1+t^2}<\mathrm{Re}(z)<-1,\\ \pi\sigma\Theta(\gamma-\gamma_{1e}), & -1<\mathrm{Re}(z)<1,\\ 0, & \mathrm{Re}(z)\ge1,\end{cases}$$

where Θ is the Heaviside function,

$$\gamma_{1e}=\frac{\mathrm{Re}(z)t+\sqrt{t^2+1-\mathrm{Re}(z)^2}}{1-\mathrm{Re}(z)^2},$$

$$\gamma_{2e}=\frac{\mathrm{Re}(z)t-\sqrt{t^2+1-\mathrm{Re}(z)^2}}{1-\mathrm{Re}(z)^2},$$

and

$$\sigma=\begin{cases}2, & \mathrm{Im}(z)<0,\\ 1, & \mathrm{Im}(z)=0,\\ 0, & \mathrm{Im}(z)>0.\end{cases}$$

For positrons, we have

$$J_{L;p}(\gamma,z,t)=\frac{1}{2}\ln\left\{\frac{\left[\mathrm{Re}(z)-S_{2p}(\gamma)\right]^2+\mathrm{Im}(z)^2}{\left[\mathrm{Re}(z)+S_{1p}(\gamma)\right]^2+\mathrm{Im}(z)^2}\right\}+i\left\{\arctan\left[\frac{S_{2p}(\gamma)-\mathrm{Re}(z)}{\mathrm{Im}(z)}\right]+\arctan\left[\frac{S_{1p}(\gamma)+\mathrm{Re}(z)}{\mathrm{Im}(z)}\right]+\theta_p(\gamma)\right\},\quad(24)$$

where

$$\theta_p(\gamma)=\begin{cases}0, & \mathrm{Re}(z)\le-1,\\ \pi\sigma\Theta(\gamma-\gamma_{1p}), & -1<\mathrm{Re}(z)\le1,\\ \pi\sigma\Theta(\gamma-\gamma_{1p})\Theta(\gamma_{2p}-\gamma), & -1<\mathrm{Re}(z)<\sqrt{1+t^2},\\ 0, & \mathrm{Re}(z)\ge\sqrt{1+t^2},\end{cases}$$

and

$$\gamma_{1p}=\frac{-\mathrm{Re}(z)t+\sqrt{t^2+1-\mathrm{Re}(z)^2}}{1-\mathrm{Re}(z)^2},$$

$$\gamma_{2p}=\frac{-\mathrm{Re}(z)t-\sqrt{t^2+1-\mathrm{Re}(z)^2}}{1-\mathrm{Re}(z)^2}.$$

Finally, using these expressions for the analytical continuation of $J_{L;j}$, we obtain a dispersion relation valid for the whole complex plane, namely,

$$\Lambda_L=1-\frac{1}{z^2}-\frac{\omega_{pe}^2\mu}{c^2k^2}+\frac{\omega_{pe}^2\mu^2}{4K_2(\mu)}\frac{1}{c^2k^2z}\times\left\{\int_1^\infty d\gamma e^{-\mu\gamma}J_{L;e}(\gamma,z,t)\left[(1-z^2)\gamma^2-2zt\gamma-(1+t^2)\right]+\int_1^\infty d\gamma e^{-\mu\gamma}J_{L;p}(\gamma,z,t)\left[(1-z^2)\gamma^2+2zt\gamma-(1+t^2)\right]\right\}=0.\quad(25)$$

From the previous definitions, it is straightforward that both functions, $J_{L;e}$ and $J_{L;p}$, are continuous and analytical in the whole complex plane (the calculation of the integrals is detailed in Appendix A). Comparing with the unmagnetized case, in the limit $t_j\to0$, we recover the solutions of Felten *et al.* in Ref. 22.

III. NUMERICAL ANALYSIS

Using the solutions (23) and (24), we can solve the dispersion relation (25). Normalizing the frequency and wave number as $x=\omega/\Omega_c$ and $y=ck/\Omega_c$, the dispersion relation (25) becomes

$$\Lambda_L=1-\frac{y^2}{x^2}-\frac{\omega_{pe}^2}{\Omega_c^2}\frac{\mu}{y^2}+\frac{\omega_{pe}^2}{\Omega_c^2}\frac{\mu^2}{4K_2(\mu)}\frac{1}{xy^3}\times\left\{\int_1^\infty d\gamma e^{-\mu\gamma}J_{L;e}(\gamma,z,t)\left[(y^2-x^2)\gamma^2-2x\gamma-(1+y^2)\right]+\int_1^\infty d\gamma e^{-\mu\gamma}J_{L;p}(\gamma,z,t)\left[(y^2-x^2)\gamma^2+2x\gamma-(1+y^2)\right]\right\}=0,\quad(26)$$

expression that is simple to solve numerically using standard computational integration methods.

In Fig. 1, we have plotted the solutions of the dispersion relation (26) for the case $\omega_{pe}/\Omega_c=1$ and various plasma temperatures: Solid (black) lines: $\mu=100$; dashed (blue) lines: $\mu=10$; dotted dashed (red) lines $\mu=5$; dotted (green) lines. $\mu=2$. Fig. 1(a) shows the real part of the normalized frequency $x=\omega/\Omega_c$ vs. the normalized wave number $y=ck/\Omega_c$. We can observe two branches that correspond to the electromagnetic ordinary and Alfvén modes. From Fig. 1(a), we can see that the electromagnetic branch has a lower frequency cutoff for the real part of the frequency, which we call the effective plasma frequency $\omega_{pe}^{\mathrm{eff}}$. The Alfvén one has an upper cutoff for the real part of the frequency, and for high temperatures, an upper cutoff for the wave number. All of these features are monotonic functions of the temperature (μ parameter). In contrast, previous models, fluid[12] and hybrid kinetic,[15] have shown that the upper cutoff for the frequency is independent of the temperature.

As seen in Fig. 1(a), the Alfvén branch presents a very interesting behavior, namely, for larger values of the wave number y the sign of $\partial\mathrm{Re}(\omega)/\partial k=\partial\mathrm{Re}(x)/\partial y$ changes. We call the region where $\partial\mathrm{Re}(x)/\partial y<0$ as anomalous zone; meanwhile, the one where $\partial\mathrm{Re}(x)/\partial y>0$ is the normal zone.

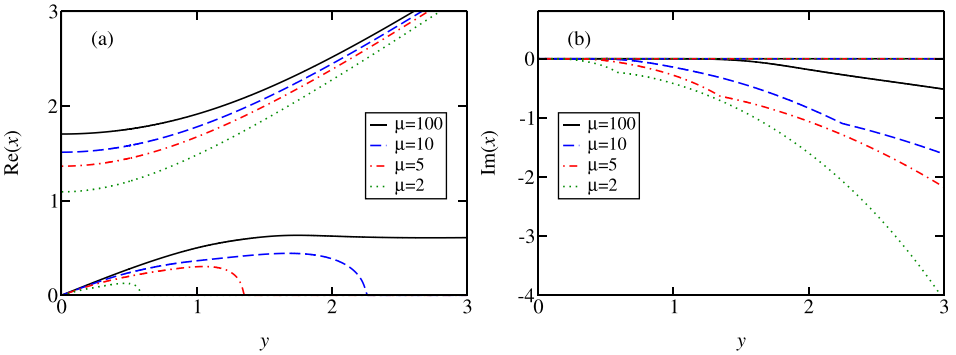

FIG. 1. Dispersion relation (26) for $\omega_{pe}/\Omega_c = 1$. (a) Normalized wave number $y = ck/\Omega_c$ vs. real part of normalized frequency $x = \omega/\Omega_c$. (b) Normalized wave number $y = ck/\Omega_c$ vs. imaginary part of normalized frequency $x = \omega/\Omega_c$. Solid (black) lines: $\mu = 100$; dashed (blue) lines: $\mu = 10$; dotted dashed (red) lines $\mu = 5$; dotted (green) lines: $\mu = 2$.

This anomalous zone appears for smaller values of y as the temperature increases (smaller μ), and as noticed above, is also characterized by the fact that there is a maximum wave number $k_{\max}$ above which the real part of the Alfvén branch vanishes. Thus, for small wavelengths, the plasma does not allow the propagation of Alfvén waves. This cutoff for the wave number decreases with the temperature, as it can be seen in Fig. 1(a). The anomalous zone in the dispersion relation of relativistic electron positron plasma has been reported earlier by Asenjo *et al.*,[12] using a relativistic fluid model, and by Domínguez *et al.*,[15] using a hybrid model in which the kinetic effects have been taken into account only along the direction of propagation of the wave. Also, the nonlinear behavior of waves belonging to this anomalous zone has been studied in recent papers, Refs. 13 and 14. However, these works have not considered kinetic damping effects on waves, which are included in this manuscript.

Fig. 1(b) shows the imaginary part of the normalized frequency vs. the normalized wave number for several temperatures. Lying on the axis $\mathrm{Im}(x) = 0$, we find four curves superimposing each other, corresponding to solutions of the electromagnetic branch for each temperature; thus, waves in this branch are stable for all wavelengths and temperatures. On the other hand, we can see that for all the temperatures considered there are solutions with $\mathrm{Im}(x) \neq 0$ corresponding to the Alfvén branch. These waves are damped due to resonant wave-particle interactions, which can be taken into account only with kinetic models. The damping increases with y and with the temperature (smaller μ). The damping rates start to increase ($\mathrm{Im}(x)$ becomes more negative) for y values in the normal zone, becomes larger in the anomalous zone and exists even after the cutoff in wave number. That is, Alfvén solutions remain after the cutoff, but correspond to aperiodic modes, where $\mathrm{Re}(x) = 0$, (see Refs. 22 and 23). Notice that the cutoff points in Fig. 1(a) correspond to the points, where the curves in Fig. 1(b) change curvature. Thus, in Fig. 1(b), such points of curvature change in the growth rate separate the regimes of periodic and aperiodic modes.

Regarding the ordinary mode, Fig. 1(a) shows that the effective plasma frequency (lower cutoff for the electromagnetic branch) decreases as we increase the temperature. Thus, as the temperature increases the plasma becomes more transparent to the propagation of light waves. This can be seen in Fig. 2(a), where we plot the normalized effective plasma frequency $x_{pe}^{\mathrm{eff}} = \omega_{pe}^{\mathrm{eff}}/\Omega_c$ vs. μ, for: Solid (black) line: $\omega_{pe}^2/\Omega_c^2 = 1$; dashed (blue) line: $\omega_{pe}^2/\Omega_c^2 = 0.5$; dotted (red) line: $\omega_{pe}^2/\Omega_c^2 = 2$. Fig. 2(b) shows the normalized Alfvén velocity v_A/c vs. μ, for the same values of ω_{pe}^2/Ω_c^2 as in Fig. 2(a). The Alfvén velocity is given by the relation $x \approx v_A y/c$, for $x \ll 1$ and $y \ll 1$. This velocity decreases with the raise of the temperature. Also, both the plasma frequency and the Alfvén speed depend on $m^{-1/2}$. Thus, relativistic effects modify the role of the thermal fluctuations through a change on the effective mass of the particles. As the temperature increases the effective mass increases, and therefore, the effective Alfvén speed and plasma frequency decrease. Both results in Fig. 2 are qualitatively consistent with the previous models of Refs. 12 and 15. From Fig. 2, we can also observe the differences between over and underdense plasmas, $\omega_{pe}/\Omega_c > 1$ or $\omega_{pe}/\Omega_c < 1$, respectively. In Fig. 2(a), it is clear that as we increase the value of ω_{pe}/Ω_c, the effective plasma frequency is increased, for all temperatures. On the other hand, Fig. 2(b) shows that the increase in ω_{pe}/Ω_c results in a decrease of the Alfvén velocity. This is an expected result, if we consider the relation $\omega_{pe}/\Omega_c = c/v_A$, in which we see that v_A is inversely proportional to ω_{pe}/Ω_c.

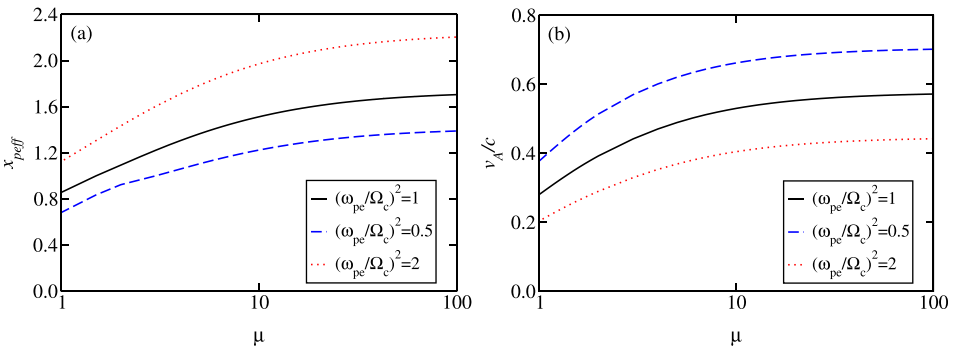

FIG. 2. (a) Normalized effective plasma frequency $x_{pe}^{\mathrm{eff}} = \omega_{pe}^{\mathrm{eff}}/\Omega_c$ vs. μ. (b) Normalized Alfvén velocity v_A/c vs. μ. Both graphs for: Solid (black) line: $\omega_{pe}^2/\Omega_c^2 = 1$; dashed (blue) line: $\omega_{pe}^2/\Omega_c^2 = 0.5$; dotted (red) line: $\omega_{pe}^2/\Omega_c^2 = 2$.

IV. PARTICLE IN CELL SIMULATIONS

To put in perspective our theoretical results we have performed a fully relativistic one dimensional full particle-in-cell (PIC) simulation, in which the momentum equation of both electrons and positrons is solved in the self-consistent electromagnetic field. In our 1.5-D (i.e., one spatial and 3 velocity dimensions) simulations, the plasma is presumed to be collisionless, homogeneous, and magnetized. The detailed description of the numerical scheme can be found in Ref. 27. We start the simulation from a quiet state, in which the particle velocities are only given by their thermal motion. The relativistic effects are included in the Lorentz equation of motion for the particles and in their thermal motion, by considering a Maxwell-Jüttner velocity distribution function for the initial condition with equal temperature and density for both electrons and positrons, so no free energy is present and the plasma is stable. The system size is $L = 512$ in units of the electron inertial length and the number of grid points is $N = 2048$, with 1000 particles per species initially in each cell. We run the simulation until $\omega_{pe}T = 1310.72$ with time steps of $\omega_{pe}\Delta t = 0.01$.

As the system evolves the initial thermal noise produces electromagnetic fields, and the normal modes of the system can be studied. We perform a two-dimensional Fourier transform (in space and time) of the magnetic field, obtaining the dispersion relation for the normal modes. In Fig. 3, we show the power spectrum for the normalized magnetic field in the case of $\omega_{pe}/\Omega_c = 1$, and $\mu = 100$ [Figs. 3(a) and 3(c)] and $\mu = 10$ [Figs. 3(b) and 3(d)], using $\omega_{pe}/\Omega_c = 1$. In this figure, we can clearly identify the normal modes described in Sec. III (Fig. 1), namely, the electromagnetic ordinary mode and the Alfvén mode. Furthermore, in the simulation results, we can see the spontaneous thermal fluctuations, which have been described in previous works for unmagnetized relativistic plasmas[22–24] and for magnetized nonrelativistic plasmas, in proton[28] and electron[29] scales. In the nonrelativistic limit, it has been shown that spontaneous fluctuations are enhanced and shifted to smaller wave numbers for higher plasma beta values,[28,29] which is consistent with our simulations. Because the relationship between the plasma beta $\beta = 8\pi n k_B T/B_0^2$ and μ is given by $\mu = (2/\beta)(\omega_{pe}^2/\Omega_c^2)$, and for $\omega_{pe}/\Omega_c = 1$, we obtain $\mu = 2/\beta$, which means that our examples correspond to $\beta = 0.02$ and 0.2, respectively. Thus, in the relativistic regime, the fluctuations are also enhanced for higher beta values. These spontaneous thermal fluctuations cannot be described by our model, because linear theory does not include fluctuations since they correspond to second order perturbations. Furthermore, the velocity distribution in Vlasov equation is an ensemble averaged quantity and does not include microscopic information as the fine-grained Klimontovich distribution.[30] We plan to study the spontaneous fluctuations in a subsequent paper.

If we focus our attention on the Alfvén branch of Fig. 3, we see that for a certain value of the normalized wave number, this branch loses its identity, and the modes with higher wave number merge with thermal fluctuations, which is consistent with the appearance of damped modes as we can see in Fig. 1(b). In the case of $\mu = 100$ (solid black line in Fig. 1), the damped modes begin to grow for $y \approx 1.5$ [see Fig. 1(b)], which is in agreement with Fig. 3(a), where the Alfvén branch becomes diffuse around $y \approx 1.5$. The same comparison can be made for $\mu = 10$, Fig. 3(b), but in this case, the wave number bandwidth for which the damped mode appears is smaller.

In Figs. 3(c) and 3(d), we present the same cases as in Figs. 3(a) and 3(b) ($\mu = 100$ and $\mu = 10$, respectively), but this time we have superimposed the dispersion relation of our kinetic model presented in Sec. III. We can see a very good match between the two approaches for both kinds of waves. For the ordinary electromagnetic mode, the agreement is better for smaller temperatures, Fig. 3(c). For larger temperatures, Fig. 3(d), the thermal fluctuations are higher and, therefore, for larger wave numbers, it is more difficult

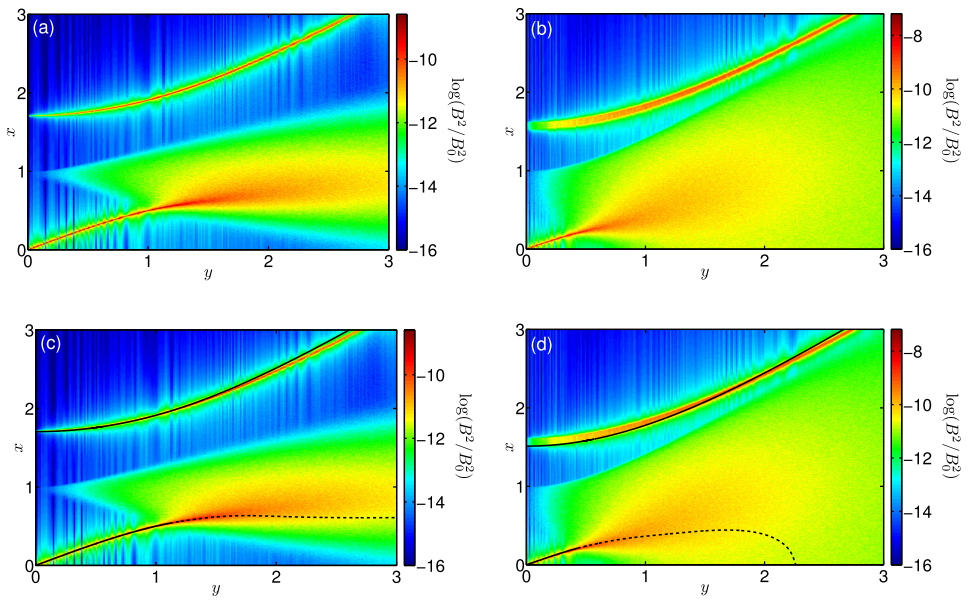

FIG. 3. Power spectrum for the normalized magnetic field fluctuations obtained from the PIC simulations. Normalized frequency $x = \omega/\Omega_c$ vs. normalized wave number $y = ck/\Omega_c$, for $\omega_{pe}/\Omega_c = 1$. (a) $\mu = 100$. (b) $\mu = 10$. (c) $\mu = 100$. (d) $\mu = 10$. Real part of numerical dispersion relation, Eq. (26), has been superimposed as a black line in Figs. (c) and (d). Solid line: numerical solution with $|\mathrm{Im}(x)| < 10^{-3}$. Dashed line: numerical solution with $|\mathrm{Im}(x)| > 10^{-3}$.

to observe the Alfvén mode from the simulations due to decreasing signal to noise ratio. However, for smaller wave numbers (normal dispersion zone), both solutions overlap. We have separated the numerical solution (black line) in two zones. The continuous black line shows the zone in which $|\mathrm{Im}(x)| < 10^{-3}$ and the dashed black line $|\mathrm{Im}(x)| > 10^{-3}$, showing the damped modes for the Alfvén branch. For smaller μ (higher β), the fluctuations tend to fill the x-y space. Thus, even though the anomalous zone begins at smaller wave number for higher temperatures, the consistent increase of thermal fluctuations does not allow us to observe a clear Alfvén branch as in the numerical solution. However, in the same wave number range, Alfvén waves become more and more damped [see Fig. 1(b)], with real frequencies approaching zero and from the theory, we also expect not to observe propagating waves at those wave numbers.

In this Section, we have restricted the study to the case $\omega_p/\Omega_c = 1$. For under and overdense plasmas, as shown in Fig. 2(a), simulations are expected to show that the electromagnetic branch is lowered with respect to Fig. 3, because the effective plasma frequency decreases. As to the Alfvén branch, simulations are expected to show that its slope at the origin decreases as ω_p/Ω_c increases [see Fig. 2(b)]. Other than this, no major differences are expected in Fig. 3 for different values of ω_p/Ω_c.

V. CONCLUSIONS

We used a full kinetic model to study the linear transverse dispersion relation for a relativistic electron-positron plasma. The correct analytical continuation for the whole frequency plane was presented. The dispersion relation was studied numerically for various plasma temperatures. We found that the dispersion relation presents two branches: the electromagnetic ordinary mode and the Alfvén mode. We have studied the main characteristics of these two branches. In the low frequency regime, the Alfvén branch presents two zones: the normal zone (where frequency increases with the wave number) and the anomalous zone (where the frequency decreases with the wave number). The existence of this anomalous zone was earlier reported in Refs. 12 and 15, in the context of a relativistic fluid theory and a one dimensional kinetic theory, respectively. In contrast to these two models, here, we found that waves in the anomalous zone of the Alfvén branch are highly damped, with the damping increasing with temperature. We also have studied the variation of Alfvén velocity and the effective plasma frequency as a function of the temperature. We obtained that relativistic effects introduce an effective mass that increases with temperature. For higher thermal motion, it is more difficult for the plasma to generate Alfvénic fluctuations (smaller effective Alfvén speed) and also the plasma becomes more transparent to the electromagnetic ordinary wave (smaller effective plasma frequency).

Finally, we have performed a fully relativistic one dimensional full particle-in-cell simulation, whose results we have compared to the dispersion relation of the model presented in this manuscript. Both results turn out to be consistent with each other, and thus the main features of the wave modes present in the simulations can be explained with the kinetic model. However, thermal spontaneous electromagnetic fluctuations are not included in the kinetic linear theory. We found that these fluctuations seem to coexist with Alfvén waves in the anomalous and aperiodic ($x = 0$) regions, where it is not possible to identify the normal mode clearly. This apparent absence of Alfvén waves in the anomalous zone during the simulations leads to the question on which effect (damping or thermal fluctuations) is more important. We plan to continue the study of this particular issue and also to extend the model for anisotropic relativistic distribution functions with free energy available to excite wave modes, which will lead us to investigate cyclotron and firehose instabilities under plasma conditions in which relativistic effects are relevant.

ACKNOWLEDGMENTS

The authors thank Roberto Navarro for useful discussions. Also, we thank the support of CONICyT through FONDECyT Grant Nos. 1110135 and 1110729 (J.A.V.); No. 1121144 (V.M.) and Postdoctoral Grant No. 3140142. (R.A.L.) We also thank the CONICyT-Becas Chile program by providing financial support for postdoctoral fellow (P.S.M.). We also thank financial support from CEDENNA. A.F.V. would like to thank the NASA-Wind/SWE project for their support.

APPENDIX A: DETAILED ANALYTICAL CONTINUATION

In this section, we follow a similar procedure used by Felten *et al.*[22] for the unmagnetized case, to calculate the appropriate analytical continuation of integral Eq. (18), whose solution has the form

$$J^{+}_{L;j} = \ln|X_j| + i\Phi\,, \tag{A1}$$

where

$$X_j = \frac{z - S_{2j}(\gamma)}{z + S_{1j}(\gamma)}\,, \tag{A2}$$

and $\Phi = \arg X_j$ is the argument of the complex function X_j, which lies in the interval $-\pi \le \arg X_j \le \pi$. S_{1j} and S_{2j} are given by the definitions Eqs. (21) and (22). We also define the complex number $z = R + iI$, where $R = \mathrm{Re}(z)$ is the real part and $I = \mathrm{Im}(z)$ is the imaginary part. Then, Eq. (A1) can be written as

$$J^{+}_{L;j} = \frac{1}{2}\ln\left[\frac{(R - S_{2j})^2 + I^2}{(R + S_{1j})^2 + I^2}\right] + i\left[\arctan\left(\frac{S_{2j} - R}{I}\right) + \arctan\left(\frac{S_{1j} + R}{I}\right)\right]. \tag{A3}$$

This solution is valid for the whole complex X_j plane, except for the points on the negative real axis, $\lim_{I\to 0^{\pm}} \mathrm{Re}(X_j) < 0$.

As the real part of X_j is given by

$$\mathrm{Re}(X_j) = \frac{(R - S_{2j})(R + S_{1j}) + I^2}{(R + S_{1j})^2 + I^2}\,, \tag{A4}$$

it follows that we have to evaluate the solution (A3) carefully when

$$\lim_{I\to 0^{\pm}} \mathrm{Re}(X_j) = \frac{R - S_{2j}(\gamma)}{R + S_{1j}(\gamma)} \le 0\,. \tag{A5}$$

There are two possible ways to satisfy the previous condition, $R - S_{2j}(\gamma) < 0$ and $R + S_{1j}(\gamma) > 0$, or $R - S_{2j}(\gamma) > 0$ and $R + S_{1j}(\gamma) < 0$. For instance, considering the first condition, the argument of X_j is

$$\Phi^{+} = \lim_{I\to 0^{+}} \Phi(R, I) = \pi\,,$$
$$\Phi^{-} = \lim_{I\to 0^{-}} \Phi(R, I) = -\pi\,,$$

therefore, there is a discontinuity as we approach from $I \to 0^{+}$ or $I \to 0^{-}$.

To solve this issue, we can impose the continuity condition for Φ

$$\lim_{I\to 0^{+}} \Phi(R, I) = \lim_{I\to 0^{-}} \Phi(R, I)\,. \tag{A6}$$

Thus, we just set

$$\Phi^{+} = \arctan\left(\frac{S_{2j} - R}{I}\right) + \arctan\left(\frac{S_{1j} + R}{I}\right),$$
$$\Phi^{-} = \Phi^{+} + 2\pi\,.$$

For the second condition, we can carry out a similar procedure. Now, Φ will be continuous in the whole complex plane, and therefore also Eq. (A3).

The two possible conditions given above to satisfy Eq. (A5) are different depending on the charge of each particle ($S_{1,j}$ and $S_{2,j}$ functions), and thus it is necessary to consider each species separately. We will examine in detail each condition as a function of γ, for both electrons and positrons.

1. Solution for electrons

Equation (A3) for electrons is

$$J^{+}_{L;e} = \frac{1}{2}\ln\left[\frac{(R - S_{2e})^2 + I^2}{(R + S_{1e})^2 + I^2}\right] + i\left[\arctan\left(\frac{S_{2e} - R}{I}\right) + \arctan\left(\frac{S_{1e} + R}{I}\right)\right], \tag{A7}$$

where

$$S_{1e}(\gamma) = \sqrt{1 - \gamma^{-2}} + \frac{t}{\gamma}\,, \tag{A8}$$

$$S_{2e}(\gamma) = \sqrt{1 - \gamma^{-2}} - \frac{t}{\gamma}\,. \tag{A9}$$

We will study only the case $t > 0$, because due to the symmetry, for $t < 0$ in the electron regime, the integral Eq. (18) becomes the one for the positrons, which we will study later (Sec. A 2). We note that $S_{1e}(\gamma) > 0$ for $t > 0$. We must focus our attention in cases that satisfy the condition in Eq. (A5), which for electrons are

$$R - S_{2e}(\gamma) < 0 \quad \text{and} \quad R + S_{1e}(\gamma) > 0\,, \tag{A10}$$

or

$$R - S_{2e}(\gamma) > 0 \quad \text{and} \quad R + S_{1e}(\gamma) < 0\,. \tag{A11}$$

The second condition, Eq. (A11), implies that $\sqrt{1 - \gamma^{-2}} < -\sqrt{1 - \gamma^{-2}}$, which is not possible, so, we will focus our attention in the first one, Eq. (A10). This condition can be written as

$$-S_{1e}(\gamma) < R < S_{2e}(\gamma)\,, \tag{A12}$$

which means that R should be in the integration interval. In Fig. 4, we plot the limits of the integration interval $-S_{1e}(\gamma)$ and $S_{2e}(\gamma)$ as a function of γ, for $t > 1$ [Fig. 4(a)] and $0 < t < 1$ [Fig. 4(b)], as in Ref. 19.

From Fig. 4, we note that we should seek the interval of γ, which satisfies the condition in Eq. (A12). For instance, for $-1 < R < 1$ and $t > 1$ [Fig. 4(a)], the condition in Eq. (A12) is fulfilled only for values of $\gamma \ge \gamma_{1e}$, i.e., R is in the integration interval $[-S_{1e}, S_{2e}]$ when $\gamma \ge \gamma_{1e}$, where γ_{1e} is solution of $R = S_{2e}(\gamma)$. However, when $-t < R < -1$, γ will be bounded by two values, the lower limit given by the solution $R = S_{2e}(\gamma)$ and the upper limit from $R = -S_{1e}(\gamma)$. Finally, for $-\sqrt{1 + t^2} < R < -t$, the limits will be given by the two solutions of $R = -S_{1e}(\gamma)$.

For $t < 1$, Fig. 4(b), we follow a similar procedure, analyzing the different cases shown in Fig. 4(a). So, identifying all the possible cases in which $\lim_{I\to 0^{\pm}} \Re X_j < 0$, we can find a general expression for the integral $J_{L;e}$. The analytical continuation for the electrons is

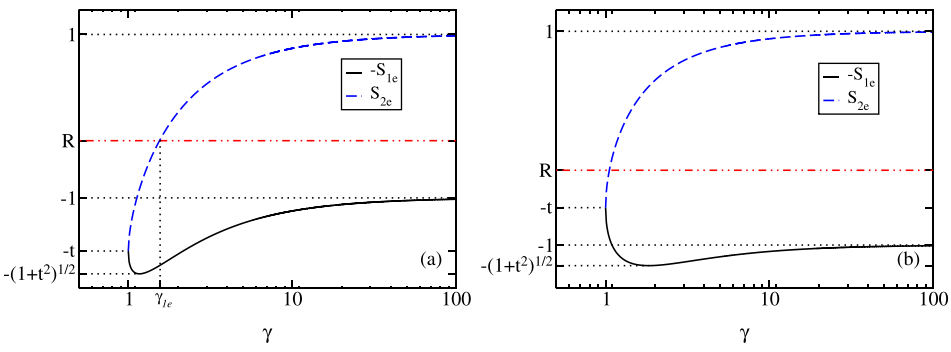

FIG. 4. Limits of the integral interval $-S_{1e}(\gamma)$ and $S_{2e}(\gamma)$, for: (a) $t > 1$; (b) $t < 1$. Solid line (black): $-S_{1e}$. Dashed line (blue): S_{2e}. Dotted dashed line (red) is a particular value of R.

$$J_{L;e}(\gamma,z,t)=\frac{1}{2}\ln\left[\frac{(R-S_{2e})^2+I^2}{(R+S_{1e})^2+I^2}\right]+i\left[\arctan\left(\frac{S_{2e}-R}{I}\right)+\arctan\left(\frac{S_{1e}+R}{I}\right)+\theta_e\right], \tag{A13}$$

with

$$\theta_e=\begin{cases}0, & R\le-\sqrt{1+t^2}\,,\\ \pi\sigma\Theta(\gamma-\gamma_{1e})\Theta(\gamma_{2e}-\gamma), & -\sqrt{1+t^2}<R<-1\,,\\ \pi\sigma\Theta(\gamma-\gamma_{1e}), & -1<R<1\,,\\ 0, & R\ge 1\,,\end{cases}$$

where Θ is the Heaviside step function,

$$\gamma_{1e}=\frac{Rt+\sqrt{t^2+1-R^2}}{1-R^2}\,,$$
$$\gamma_{2e}=\frac{Rt-\sqrt{t^2+1-R^2}}{1-R^2}\,,$$

and

$$\sigma=\begin{cases}2, & I<0\,,\\ 1, & I=0\,,\\ 0, & I>0\,.\end{cases}$$

This function is continuous and analytical in the whole complex plane, so we have omitted the upper index + in $J_{L;e}$.

2. Solution for positrons

Equation (A3) for positrons is

$$J^{+}_{L;p}=\frac{1}{2}\ln\left[\frac{(R-S_{2p})^2+I^2}{(R+S_{1p})^2+I^2}\right]+i\left[\arctan\left(\frac{S_{2p}-R}{I}\right)+\arctan\left(\frac{S_{1p}+R}{I}\right)\right], \tag{A14}$$

where

$$S_{1p}(\gamma)=\sqrt{1-\gamma^{-2}}-\frac{t}{\gamma}\,, \tag{A15}$$

$$S_{2p}(\gamma)=\sqrt{1-\gamma^{-2}}+\frac{t}{\gamma}\,. \tag{A16}$$

As in the previous case, we will consider only $t>0$. The condition (A5) gives us the cases

$$R-S_{2p}(\gamma)<0 \quad \text{y} \quad R+S_{1p}(\gamma)>0\,, \tag{A17}$$

or

$$R-S_{2p}(\gamma)>0 \quad \text{y} \quad R+S_{1p}(\gamma)<0\,. \tag{A18}$$

As in Sec. A 1, the second condition, Eq. (A18), is not fulfilled for any values of γ and t. The first one can be written as

$$-S_{1p}(\gamma)<R<S_{2p}(\gamma). \tag{A19}$$

In Fig. 5, we can see the behavior of the functions $-S_{1p}$ and S_{2p} as a function of γ, for $t>1$ [Fig. 5(a)] and $t<1$ [Fig. 5(b)].

As in the electron case, we will study all the cases shown in Fig. 5, obtaining the solution

$$J_{L;p}(\gamma,z,t)=\frac{1}{2}\ln\left[\frac{(R-S_{2p})^2+I^2}{(R+S_{1p})^2+I^2}\right]+i\left[\arctan\left(\frac{S_{2p}-R}{I}\right)+\arctan\left(\frac{S_{1p}+R}{I}\right)+\theta_p\right], \tag{A20}$$

with

$$\theta_p=\begin{cases}0, & R\le-1\,,\\ \pi\sigma\Theta(\gamma-\gamma_{1p}), & -1<R\le 1\,,\\ \pi\sigma\Theta(\gamma-\gamma_{1p})\Theta(\gamma_{2p}-\gamma), & -1<R<\sqrt{1+t^2}\,,\\ 0, & R\ge\sqrt{1+t^2}\,,\end{cases}$$

where Θ is the Heaviside step function,

$$\gamma_{1p}=\frac{-Rt+\sqrt{t^2+1-R^2}}{1-R^2}\,,$$
$$\gamma_{2p}=\frac{-Rt-\sqrt{t^2+1-R^2}}{1-R^2}\,,$$

and

$$\sigma=\begin{cases}2, & I<0\,,\\ 1, & I=0\,,\\ 0, & I>0\,.\end{cases}$$

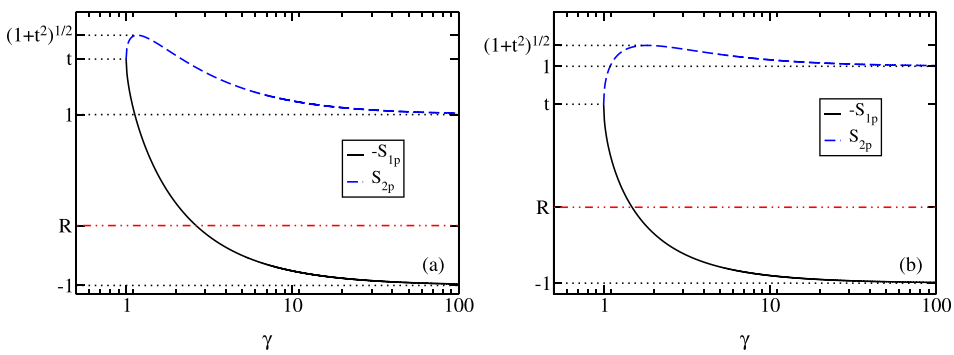

FIG. 5. Limits of the integral interval $-S_{1p}(\gamma)$ and $S_{2p}(\gamma)$, for: (a) $t>1$; (b) $t<1$. Solid line (black): $-S_{1p}$. Dashed line (blue): S_{2p}. Dotted dashed line (red) is a particular value of R.

This function is continuous and analytical in the whole complex plane.

[1]E. P. T. Liang, Astrophys. J. **234**, 1105 (1979).
[2]T. R. White and A. P. Lightman, Astrophys. J. **340**, 1024 (1989).
[3]G. Björnsson, M. A. Abramowicz, X. Chen, and J.-P. Lasota, Astrophys. J. **467**, 99 (1996).
[4]*In The Very Early Universe*, edited by G. W. Gibbons, S. Hawking, and S. T. C. Siklos (Cambridge University Press, Cambridge, 1985).
[5]T. Tajima and T. Taniuti, Phys. Rev. A **42**, 3587 (1990).
[6]M. F. Curtis, *The Theory of Neutron Stars Magnetospheres* (University of Chicago Press, Chicago, 1991).
[7]Y. N. Istomin and D. N. Sobyanin, Astron. Lett. **33**, 660 (2007).
[8]V. V. Usov, Phys. Rev. Lett. **80**, 230 (1998).
[9]D. B. Blaschke, A. V. Prozorkevich, C. D. Roberts, S. M. Schmidt, and S. A. Smolyansky, Phys. Rev. Lett. **96**, 140402 (2006).
[10]G. P. Zank and R. G. Greaves, Phys. Rev. E **51**, 6079 (1995).
[11]P. Helander and D. J. Ward, Phys. Rev. Lett. **90**, 135004 (2003).
[12]F. A. Asenjo, V. Muñoz, J. A. Valdivia, and T. Hada, Phys. Plasmas **16**, 122108 (2009).
[13]R. A. López, F. A. Asenjo, V. Muñoz, and J. A. Valdivia, Phys. Plasmas **19**, 082104 (2012).
[14]R. A. López, F. A. Asenjo, V. Muñoz, A. C.-L. Chian, and J. A. Valdivia, Phys. Rev. E **88**, 023105 (2013).
[15]M. Domínguez, V. Muñoz, and J. A. Valdivia, Phys. Rev. E **85**, 056416 (2012).
[16]V. Muñoz and L. Gomberoff, Phys. Plasmas **9**, 2534 (2002).
[17]V. Muñoz, Phys. Plasmas **11**, 3497 (2004).
[18]R. Schlickeiser, Phys. Scr. **1998**, 33.
[19]M. Lazar and R. Schlickeiser, Can. J. Phys. **81**, 1377 (2003).
[20]M. Lazar and R. Schlickeiser, New J. Phys. **8**, 66 (2006).
[21]R. Schlickeiser and P. H. Yoon, Phys. Plasmas **19**, 022105 (2012).
[22]T. Felten, R. Schlickeiser, P. H. Yoon, and M. Lazar, Phys. Plasmas **20**, 052113 (2013).
[23]T. Felten and R. Schlickeiser, Phys. Plasmas **20**, 082116 (2013).
[24]T. Felten and R. Schlickeiser, Phys. Plasmas **20**, 082117 (2013).
[25]R. Schlickeiser, Phys. Plasmas **17**, 112105 (2010).
[26]F. Jüttner, Ann. Phys. **339**, 856 (1911).
[27]R. A. López, V. Muñoz, A. F. Viñas, and J. A. Valdivia, Phys. Plasmas **21**, 032102 (2014).
[28]J. A. Araneda, H. Astudillo, and E. Marsch, Space Sci. Rev. **172**, 361 (2012).
[29]A. F. Viñas, P. S. Moya, R. Navarro, and J. A. Araneda, Phys. Plasmas **21**, 012092 (2014).
[30]S. Ichimaru, *Statistical Plasma Physics, Volume I: Basic Principles*, Frontiers in Physics (Addison-Wesley, 1992).